



OPEN

Nano-porous architecture of N-doped carbon nanorods grown on graphene to enable synergetic effects of supercapacitance

SUBJECT AREAS:
ELECTRONIC PROPERTIES
AND DEVICES
BATTERIES

Received
24 March 2014

Accepted
19 November 2014

Published
18 December 2014

Correspondence and
requests for materials
should be addressed to
N.Z. (zhaoning@
iccas.ac.cn); J.X. (jxu@
iccas.ac.cn) or F.P.
(panfeng@pkusz.edu.
cn)

H. S. Fan^{1,2}, H. Wang¹, N. Zhao¹, J. Xu¹ & F. Pan²

¹Beijing National Laboratory for Molecular Sciences, Laboratory of Polymer Physics and Chemistry, Institute of Chemistry, Chinese Academy of Sciences, Beijing 100190, P.R. China, ²School of Advanced Materials, Peking University Shenzhen Graduate School, Shenzhen, 518055, P. R. China.

A novel nano-porous 3D architecture of N-doped carbon nanorods arrays grown on the surface of graphene has been prepared by carbonizing polyaniline/graphene oxide (PANI-GO) composite with PANI nanorod arrays on both sides of GO nanosheets. The obtained carbon materials are entirely composed of regularly grown carbon nanorods on graphene with height of about 100 nm and width about 30 nm, showing porous property due to the decomposition of PANI chains. The morphology of PANI grown on GO at the different growth stages was investigated to demonstrate the mechanism of the finally hierarchical architecture formation. Due to its large specific surface area and incorporation of the nitrogen groups into the carbon matrix, the obtained 3D carbon material enhances the ionic transport and the super-capacitance by synergetic effect of both double-layer and faradaic capacitances. This study provides a controllable approach to fabricate hierarchical carbon material based on conducting polymers and graphene oxide with promising applications in the high-rate electrode material of supercapacitors.

As an important energy storage device, supercapacitor has attracted great research interests due to its combination of the high power of dielectric capacitor and the high specific energy of rechargeable battery, which can be used in hybrid electric vehicles, uninterrupted power supplies, digital communication devices, and other high-power apparatuses^{1–3}. Carbon materials^{4,5}, transition metal oxides^{6,7}, and conducting polymers^{8,9} have been widely used as electrode materials for supercapacitor owing to their prominent capacitive properties. Among these attractive electrodes, transition metal oxides and conducting polymers have high specific capacitance, but their applications are limited by their high cost, poor chemical reversibility and lack of cycling stability in aqueous electrolytes^{10,11}. Carbon materials have been considered as promising electrode materials due to their chemical stability, low cost, high conductivity and wide applications^{12,13}. Conventional carbon materials, such as carbon nanotubes and carbon fibers, show low gravimetric capacitances, which limit their practical application. Therefore, it is a considerable challenge for searching and exploiting new carbon material with low cost and high capacity.

In recent years, conducting polymers, specially polyaniline (PANI) has been widely used as an attractive precursor for the synthesis of carbon material due to its ease of synthesis, low cost and chemical and environmental stability. The transformation of PANI into porous carbon can effectively introduce nitrogen groups into the carbon matrix, which gives carbon materials an acid/base character and enhances the capacitance by the synergetic effect of both double-layer and faradaic capacitance^{14–19}. Generally, the specific capacitance of carbon materials can be improved by increasing the specific surface area with hierarchical and porous structures by enhancing the electronic transport in the electrodes or at the interface of the electrode/electrolyte¹². Therefore, nanostructured electrodes with porous morphology and good electrical conductivity are desirable²⁰. Focusing on this aim, hierarchical carbon materials are of great advantage since they can greatly facilitate ionic motion and reduce the diffusion length, thus ensure high utilization of electrode materials and enhance the rate performance of electrode. For example, Fan and co-workers reported three-dimensional hybrid carbon nanocomposites of 1D carbon nanotubes and 2D graphene with excellent electrochemical performance²¹. Hierarchical graphene-carbon nanotube architecture has been designed for supercapacitors by Yang and co-workers²².



In this paper, we report a novel nano-porous hierarchical carbon material of porous carbon nanorods array on the surface of graphene, which is synthesized by carbonization of hierarchical PANI-GO nanocomposites. The prepared nano-porous carbon material possesses excellent electrochemical performance due to the high specific surface area and combination with nitrogen groups. The specific capacitance of the as-prepared nano-porous carbon material can reach 372 F g^{-1} in 6 M KOH aqueous solution, showing promising application in supercapacitors. This method provides a new approach to fabricate hierarchical carbon material for energy storage based on conducting polymers.

Results and Discussions

Morphology and mechanism. We demonstrate the preparation of a novel nano-porous 3D architecture of N-doped carbon nanorods grown on graphene surfaces by carbonizing the PANI-GO composite. As illustrated in Figure 1, various functional groups (e.g., carbonyl, hydroxyl, and epoxy groups) on GO surface can attach anilinium ions through the electrostatic attraction to become the nuclear site of a “seed” on GO. Due to the large specific surface area of GO, a lots of active sites are generated on the surface of the GO. As APS is added, anilinium ions begin to polymerize at the active sites to form PANI on the GO surface. To reduce the interfacial energy of the whole system, these as-formed PANI will act as “seeds” for the following polymerization, leading to that the later formed PANI grow around the seeds. The PANI polymer traces will be grown on the seeds step by step along vertical directions with the polymerization time. As a result, PANI nanorod arrays vertically aligned on the GO surface are formed. In parallel, the π - π stacking force between the graphitic structure of GO and the aromatic rings of PANI will also contribute to induce the polymerization along horizontal directions occurring on the surface of GO. In our case free PANI nanofibers are not likely formed in the bulk solution owing to the low concentration of aniline and the plenty of oxygen-containing functional groups and large specific area of GO²⁵. The hierarchical 3D PANI-GO structure can be remained after carbonizing, leading to the final N-doped carbon materials of carbonized PANI-GO (named as CPG). It is the decomposition of PANI chains (C-N, C-H and N-H bonds) in the nitrogen atmosphere results in the formation of N-doped porous carbon nanorods on the surface of graphene.

Typical SEM and TEM images of the obtained PANI-GO and CPG are shown in Figure 2. PANI-GO composites with a uniform

hierarchical structure have been successfully prepared (Figure 2a). From the high resolution SEM image in Figure 2b, it can be observed that a great many of thorn-like PANI nanorods are formed vertically on the surface of GO. The PANI nanorods cover on both sides and the edges of GO to form a shell, while the vertical PANI nanorods have an average length of 100 nm and diameter in the middle height of 30 nm . TEM image reveals PANI nanorod arrays on the surface of GO are regular and uniform (Figure 2c). After carbonizing the PANI-GO, it can be obtained that the final CPG hierarchical carbon materials with the porous carbon nanorods array vertically aligned on the surfaces and the edges of graphene sheets (Figure 2d, e and f).

In order to further understand morphology evolution and formation mechanism of the hierarchical composites, products of PANI-GO at different reaction times were taken out of the reaction solution and monitored by SEM. As shown in Figure 3a, a few tiny protuberances, which are the polymer seeds, are formed on the surface of the GO after the reaction of 1 h , which is different from the smooth surface of pure GO. When the polymerization time extends to 2.5 and 4.5 h , the size and height of PANI protuberances, increase step by step (Figure 3b and 3c). It seems that further polymerization leads to the growth and aggregation of the adjacent smaller protuberances to form the large PANI nanorods. At last, aligned PANI nanorod arrays are formed vertically along the surface of GO (Figure 3d). The functional groups on the GO surface and the π - π stacking force between the graphene parts of the GO and the aromatic rings of PANI contribute to the formation of the hierarchically structured PANI-GO composites.

Chemical structure characterization. Figure 4 presents UV-vis spectra of the samples in aqueous solutions. Pure GO and the obtained CPG have no obvious absorption (Figure 4a and 4b). Doped PANI-GO (Figure 4c) shows two peaks centered at about 440 and 820 nm , attributing to benzenoid rings and quinoid rings, respectively. It is indicated that they are in emeraldine salt form of PANI, corresponding to the suspension of light green (inset c). After being dedoped with 0.5 M ammonium hydroxide, the absorption of dedoped PANI-GO (Figure 4d) exhibits obvious blue shift compared with that of the doped counterparts. The color of the suspension also changes into light blue (inset d), suggesting the emeraldine base form of PANI. Besides, the quinoid (Q)/benzenoid (B) ratio of the dedoped PANI-GO decreases significantly in contrast to the doped PANI-GO, demonstrating that more reduced leucoemeraldine segments exist in the dedoped state.

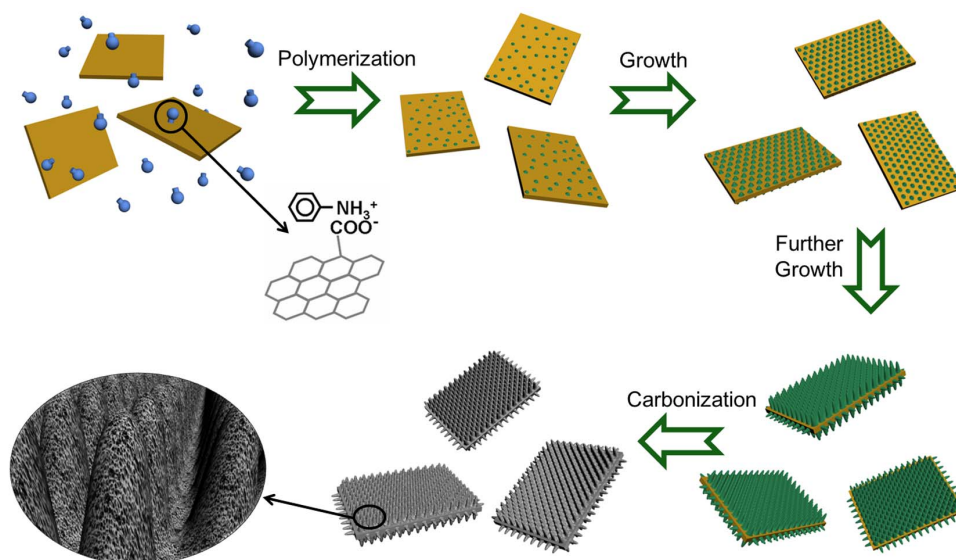


Figure 1 | Schematic of the formation of the hierarchical CPG materials with N-doped carbon nanorods on graphenes.

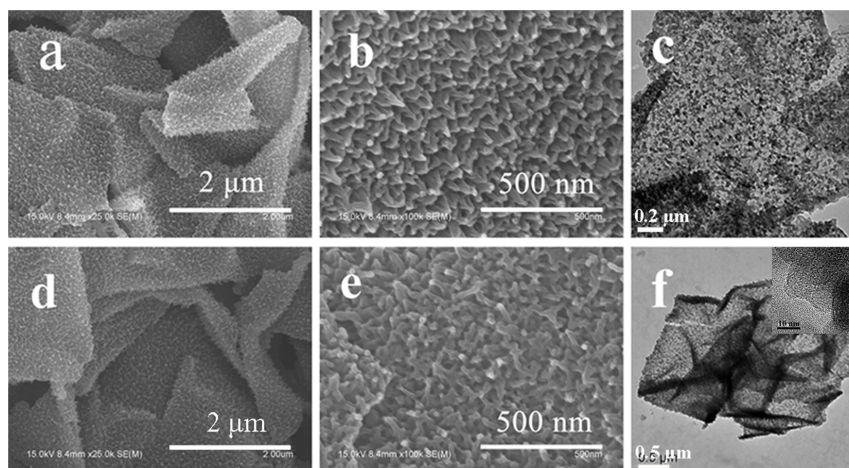


Figure 2 | SEM and TEM images of the PANI-GO (a, b and c) and CPG (d, e and f) (Inset of f shows porous carbon structures).

FTIR spectra of the samples are shown in Figure 5a. For GO, the main peaks around 3399 , 1729 and $1391\text{--}1060\text{ cm}^{-1}$ are attributed to the O-H, C=O in COOH, and C-O in C-OH/C-O-C functional groups, respectively²³. The obtained PANI-GO composites exhibit similar characteristic peaks as compared to the pure PANI. The main absorption bands centered at 1566 and 1485 cm^{-1} can be ascribed to C=C stretching vibration of the quinoid ring and the benzenoid ring in PANI, suggesting the presence of the emeraldine salt state of PANI. The peaks at 1299 , 1246 , 1145 and 818 cm^{-1} are attributed to the C-N stretching vibration of the benzene ring, stretching vibration of the CN^+ in the polaron structure of PANI, stretching of C=N ($-\text{N}=\text{quinoid}=\text{N}-$) and out of plane bending vibration of C-H in benzene ring, respectively. The resulting CPG shows almost no absorption peaks.

Figure 5b presents the XRD patterns. The typical peaks of diffractogram of GO centered at $2\theta = 12.1^\circ$ is observed, corresponding to the (002) inter-planar spacing of 0.73 nm . For pure PANI, the crystalline peaks centered at about 20° and 25° can be assigned to (020) and (200) reflections of PANI in its emeraldine salt form. The XRD patterns of PANI-GO exhibits similar crystal peaks compared with that of PANI, revealing a similar crystalline of the PANI nanorods to that of the pure PANI. The results suggest that no additional crystalline order is introduced into the obtained composites in the presence of GO. The XRD pattern of CPG exhibits two broad diffraction

peaks around 25° and 44° , which correspond to the (002) and (100) facets of the hexagonal graphitic carbon, respectively²⁴.

XPS (Figure 5c) is used to measure the elemental composition on the surface and confirm the nitrogen doping onto the CPG. The survey spectrum shows that GO consist of oxygen (531 eV) and carbon (285 eV). The content of O element of GO is of 29.1% , as shown in Table 1, indicating the existence of plenty of oxygenous functional groups. PANI-GO displays additional nitrogen group (399 eV) by the PANI nanorods on the surface of GO. After the carbonization of PANI-GO, The C element content increases but the O and N element contents decrease due to the removal of light molecules and gases generated by the cracking reaction of PANI chains during carbonization. CPG also exhibits the N element at 399 eV with the content of 8.2% , indicating the nitrogen doping on the CPG. It is expected that the combination with the nitrogen groups can greatly improve the electrochemical performance of CPG electrode by pseudocapacitive effect.

Raman spectroscopy was used to analyze the microstructure of GO, PANI-GO and CPG here. As shown in Figure 5d, the broad D band at 1345 cm^{-1} and G band at 1584 cm^{-1} are attributed to the conversion of a sp^2 -hybridized carbon to a sp^3 -hybridized carbon and the in-plane bond-stretching motion of the pairs of C sp^2 atoms, respectively. For PANI-GO, there are few new peaks at 1514 , 1176 , 1036 and 880 cm^{-1} were attributed to C=C stretching, C-H bending vibration of the benzenoid ring, N-H bending in-plane of the benzenoid ring and C-N-C wag out-of-plane of the benzenoid ring,

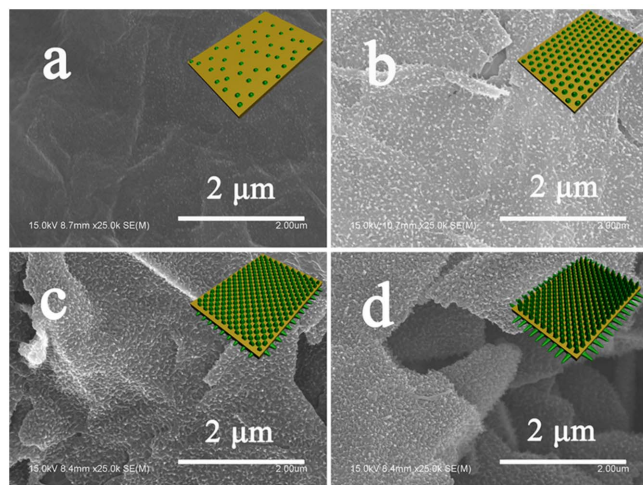


Figure 3 | SEM images of PANI-GO synthesized at different polymerization times: (a) 1 h; (b) 2.5 h; (c) 4.5 h; (d) 9 h.

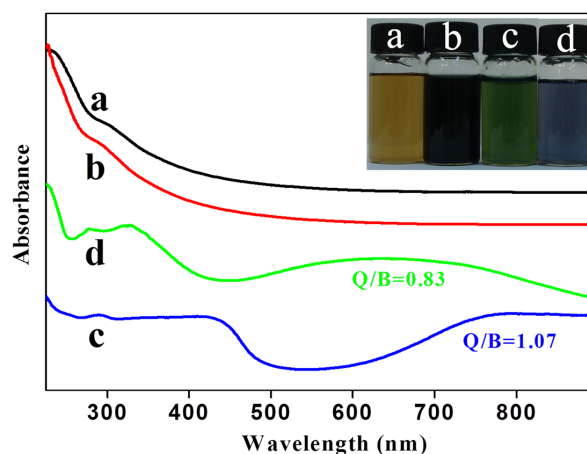


Figure 4 | UV-vis spectra of (a) GO, (b) CPG, (c) doped PANI-GO and (d) dedoped PANI-GO. Inset is the photo of the aqueous dispersions of (a-d).

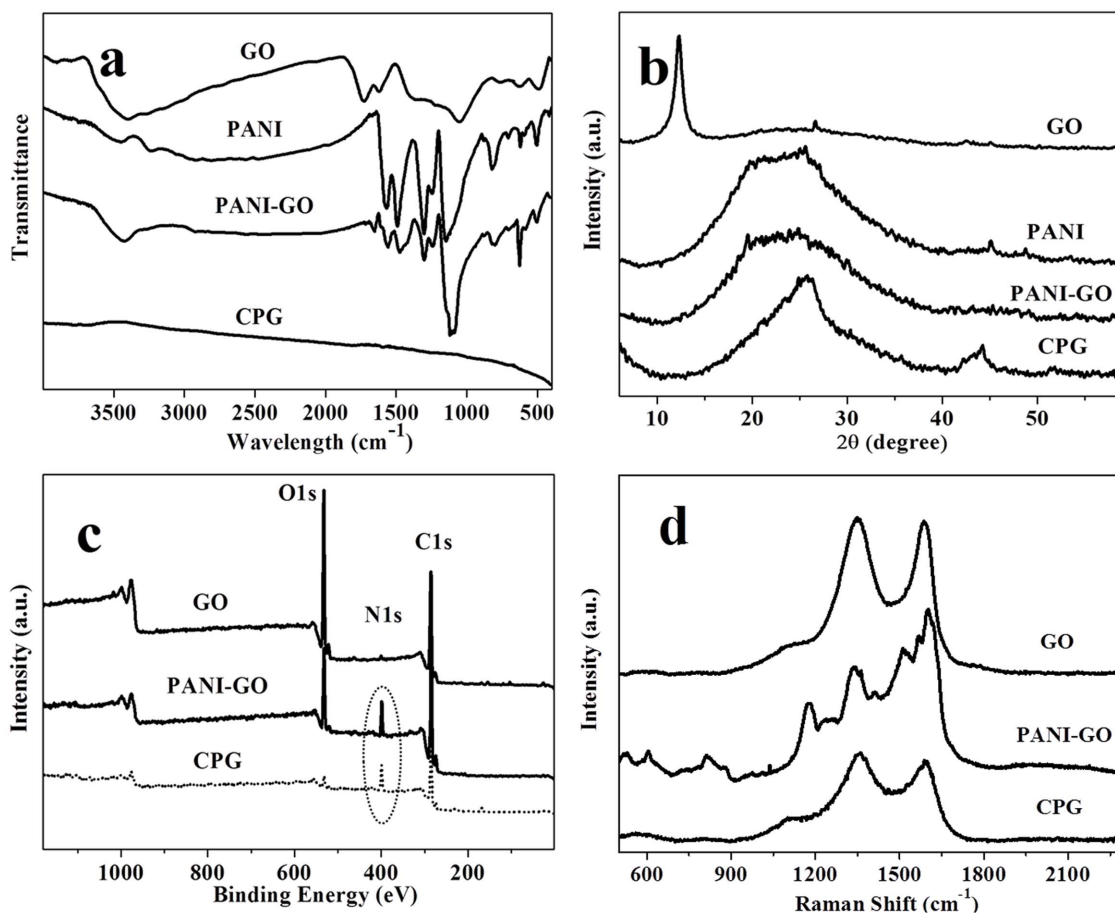


Figure 5 | FTIR (a), XRD (b), XPS (c) and Raman (d) spectra of all samples.

respectively. The carbonized CPG exhibit similar Raman peaks of GO with obvious D band and G band, which is further demonstrate the full transformation of PANI-GO into carbon materials.

The N_2 adsorption-desorption isotherms are further used to investigate the effect of carbonization on the microstructure and exposed surface area in the nano-porous materials. As shown in Figure 6, PANI-GO and CPG are found to yield a pseudotype-I curve with H_1 hysteresis loop at high relative pressure between 0.8 and 1.0, confirming the presence of nano-porous, micropores and mesopores architectures²⁵. The adsorption isotherms of the both samples become rapidly saturated at low relative pressure, which illustrates the adsorption of micropores. From a comparison of the two curves, CPG shows a higher initial leap at low pressure and a continuous increase of adsorption capacity in a wide pressure range. The increase of adsorption capacity at low pressure is mainly related to the micropores, while the increase of the adsorption capacity with increasing pressure is attributed to the presence of high mesopore distribution after carbonization. Meanwhile, the surface area of the CPG ($216 \text{ m}^2 \text{ g}^{-1}$) increases after being carbonized in comparison to PANI-GO ($73 \text{ m}^2 \text{ g}^{-1}$), showing increased surface area due to the formation of micro and mesopores on the carbon nanorods from the decomposition of PANI chains in the carbonation process. Therefore, the hier-

archical carbon material prepared has an increased surface area, which benefits the electrolyte ionic transport from the bulky solution to the surface of CPG. Thus good electrochemical performance can be expected.

Electrochemical characterization. The electrochemical performance of the electrode materials was characterized by cyclic voltammograms (CV). The CV curves of the CPG electrode at the scan rates of 5, 25 and 100 mV s^{-1} are shown in Figure 7a. The curves present a quasi-rectangle in shape along the potential-current axis without obvious redox peaks, which indicate that CPG electrode has ideal capacitive behavior²⁶. Besides, the current density obviously increases by increasing scan rates with almost no distortion in the CV curves at higher scan rates of 100 mV S^{-1} , implying a good rate capability for the CPG electrode and good stability at wide scan rate ranges. The good electrochemical performance of CPG electrode suggests that it can be a good candidate as electrode material for supercapacitor.

EIS is an important tool to obtain information of frequency dependence, equivalent series resistance (ESR) and charge transport at the material/electrolyte interface for supercapacitor electrode. Figure 7b illustrates the Nyquist plot of the CPG electrode. A semi-circle of small radius is obtained at high-frequency region and a straight line in the low frequency region, corresponding to electron-transfer-limited process and diffusional-limited electron-transfer process²⁷, respectively. The intercept at the real axis at high frequencies is the ESR value of about 1.3Ω for CPG electrode, showing good electric conductivity. The imaginary part of the impedance spectra at low frequencies represents the capacitive behavior of the electrode and approaches a vertical line in an ideal capacitor²⁸. Obviously, the straight line part of CPG is close to vertical line along

Table 1 | The element components of GO, PANI-GO and CPG

Sample	C	O	N
GO	69.9	29.1	—
PANI-GO	74.9	14.4	10.7
CPG	90.7	1.1	8.2

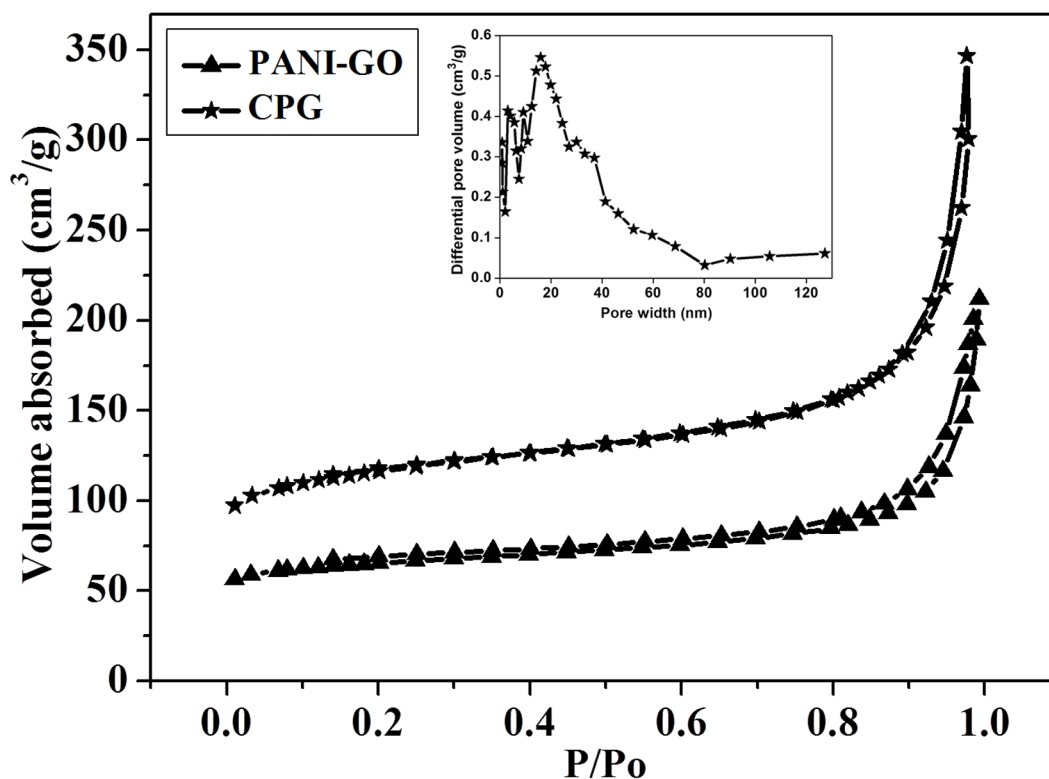


Figure 6 | N_2 adsorption/desorption isotherms of PANI-GO and CPG (Inset shows pore size distribution of CPG).

the imaginary axis, suggesting this hierarchical carbon material has excellent capacitive behavior.

Figure 7c gives the charge/discharge curves of CPG electrode material at different current densities within a potential window -0.8 to 0.2 V vs. SCE. The charge/discharge curve of CPG electrode shows a quasi-triangular shape which is a characteristic of electrical double-layer capacitance. The curves keep similar shapes in the potential range of -0.8 – 0.2 V at the densities from 1.0 to 0.1 A g^{-1} , revealing that the carbon material can experience a wide range of current. Meanwhile, the charge/discharge duration of the CPG electrode increases with the decreasing of current density from 1.0 to 0.1 A g^{-1} . It indicates that the charge/discharge duration is proportional to the current density. Furthermore, the discharge time is longer than the charge time as the current density decreases, which is probably attributed to the interaction between CPG and electrolyte ions at lower current density. The specific capacitance is calculated according to the equation $C_m = C/m = It/\Delta Vm^{29}$, where C_m is the specific capacitance ($F g^{-1}$), I is the charge/discharge current, t is the time of discharge, ΔV is the voltage difference between the upper and lower potential limits, and m is the mass of active material. The specific capacitance of CPG is $372 F g^{-1}$ at a current density of 0.1 A g^{-1} , and it is 314 , 273 and $201 F g^{-1}$ at current densities of 0.2 , 0.5 and 1 A g^{-1} , respectively, demonstrating a better storage capacity of energy at low current density to indicate the synergetic effect of both double-layer and faradaic capacitances. In comparison, it can be noted that the specific capacitance of CPG ($372 F g^{-1}$) is larger than that of C-graphene ($170 F g^{-1}$)¹³, PANI-based carbon nanorods ($327 F g^{-1}$)³⁰, PANI-based activated carbon ($210 F g^{-1}$)³¹, PANI-based carbon nanotubes ($163 F g^{-1}$)³² and graphene-carbon nanotube ($326.5 F g^{-1}$)²². The greatly improved specific capacitance is mainly due to the novel nano-porous hierarchical structures of CPG and the incorporation of the nitrogen groups. The hierarchical structure with porous carbon nanorods grown on the surface of graphene effectively increases its specific surface area and thus benefits the ion diffusion from the bulky solution to the surface of electrode material. Meanwhile, the combination with nitrogen

groups can greatly enhance the electrochemical performance of CPG electrode by pseudocapacitive effect.

To evaluate the electrochemical stability, repeating consecutive charge/discharge cycles at a current density of 1 A g^{-1} were employed (Figure 7d). Although the specific capacitance of the CPG electrode decreases with the increase of cycles, it still keeps 98.7% of its initial capacitance after 3000 consecutive cycles, exhibiting excellent long-term cyclability and high degree of reversibility in consecutive scan cycles. The good cyclic stability may attribute to its quite small ESR for the ionic diffusion and the pseudocapacitance effect introduced by nitrogen²².

Conclusions

PANI-GO composites with a well ordered hierarchical structure of PANI nanorods vertically aligned on the surface of GO were simply prepared by in situ polymerization of ANI in the presence of GO. The as-formed PANI structure on the GO surface can be simply controlled by the polymerization time. After being carbonized, nitrogen-enriched nano-porous carbon material remaining the original hierarchical morphology was obtained. Due to its nano-porous hierarchical structure with large specific surface area and incorporation of the nitrogen groups, the resultant carbon material shows higher specific capacitance by synergetic effect of both double-layer and faradaic capacitances, indicating a promising application as electrode material for supercapacitor. This study not only provides a controllable approach to fabricate hierarchical carbon material based on conducting polymers and graphene oxide, but also gives an insight for the application in electrode material for supercapacitor.

Methods

Synthesis. Firstly, 2 mg mL^{-1} graphene oxide (GO, prepared by the modified Hummers method³³) in 50 mL 1 M $HClO_4$ aqueous solution was ultrasonicated for 30 min to obtain an exfoliated yellow-brown suspension. The ANI monomer (1 mmol) was added into the above suspension and stirred for 30 min to get a uniform mixture. Then aqueous solution of 1 M $HClO_4$ containing APS (the molar ratio of ANI/APS is $1:1$) was slowly added under stirring. The polymerization of ANI was conducted at room temperature for 12 h, while the yellow-brown suspension

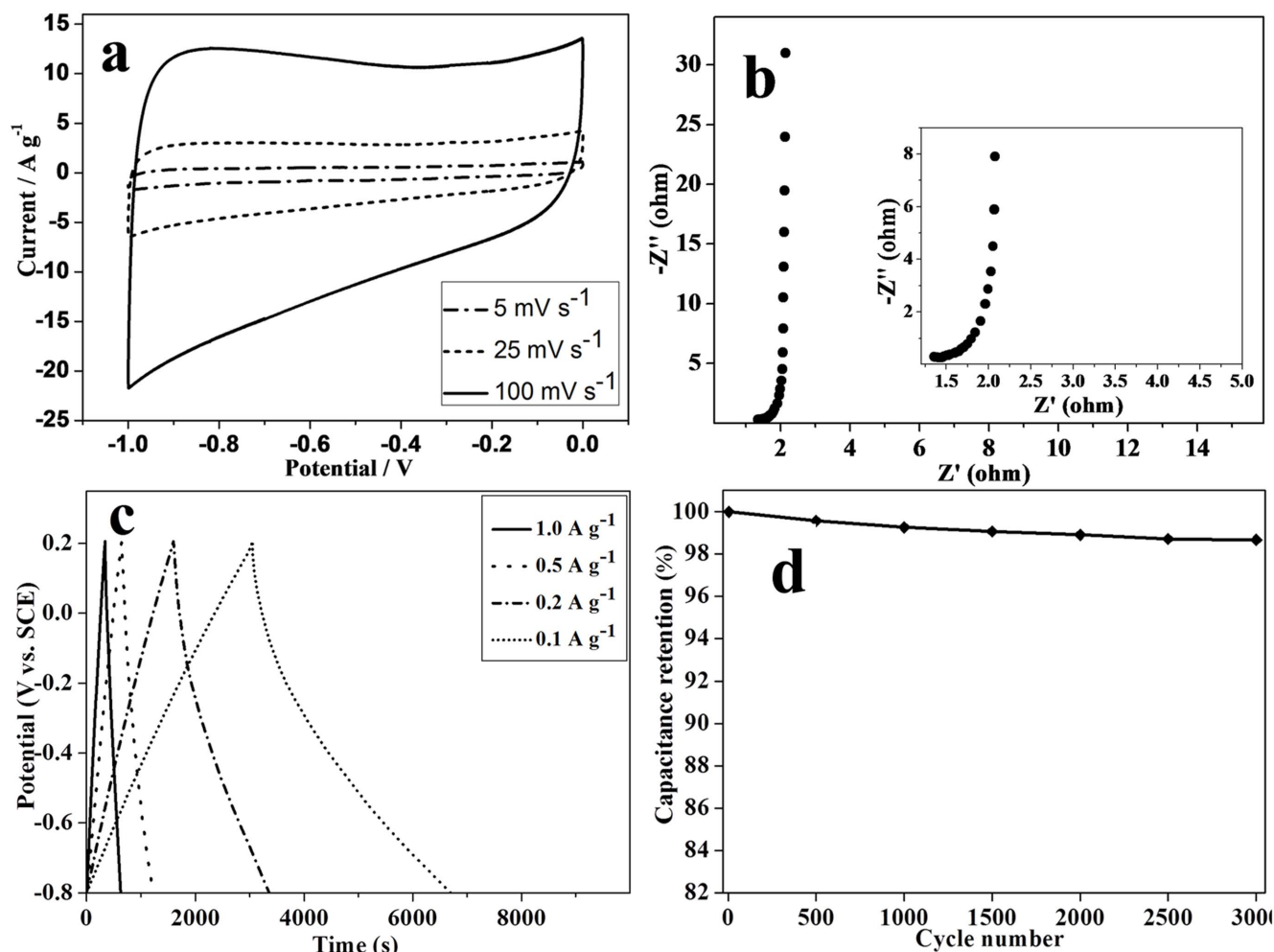


Figure 7 | (a) CV curves of CPG at different scan rates in 6 M KOH solution. (b) Nyquist plot of CPG (Inset: enlarged high-frequency region of the Nyquist plot). (c) Galvanostatic charge/discharge curves of CPG electrode at different current densities. (d) Variation of the specific capacitance of CPG electrode as a function of the cycle number.

gradually changed to deep green. The obtained products were filtered and rinsed with distilled water and signed as PANI-GO. Secondly, PANI-GO was carbonized at 850°C for 3 h under nitrogen flow and the final carbonized PANI-GO was named as CPG.

Electrochemical Characterizations. Electroactive composites, carbon black and poly (tetrafluoroethylene) in a mass ratio of 85:10:5 were well mixed to obtain homogeneous slurry. The slurry was coated and pressed on a foam nickel to prepare working electrode, and then the electrode was dried at 60°C for 24 h in a vacuum oven. Electrochemical performances of the samples were measured with a three electrode system, in which platinum foils and saturated calomel electrode (SCE) were used as counter and reference electrodes, respectively. The electrolyte is 6 M KOH aqueous solution. Cyclic voltammetry (CV) and electrochemical impedance spectroscopy (EIS) measurements were studied using a Zahner IM6 electrochemical working station. The scan voltage ranged from -1.0 to 0 V in CV measurements.

Materials Characterization. Morphology of all the products was characterized by scanning electron microscope (SEM, Hitachi S4800) and transmission electron microscope (TEM, JEOL JEM-2200FS). Fourier transform infrared (FTIR) spectra were recorded on a Bruker Equinox 55 spectrometer in the range of 400–4000⁻¹ cm at room temperature. UV-vis spectra were measured on a Shimadzu 1601PC UV-vis spectrophotometer. X-ray diffraction (XRD) experiment was carried out on a Micscience M-18XHF (with CuK α radiation) instrument. X-ray photoelectron spectroscopy (XPS) analysis was carried out on an ESCALab220i-XL electron spectrometer from VG Scientific. Al-K α radiation was used as the X-ray source and operated at 300W. Pore structure of the samples was characterized by physical adsorption of N₂ at 77 K (TriStar II 3020). The surface specific area was obtained by the Brunauer Emmett Teller method. Raman spectra were studied from a LabRAM HR800 with a 532 nm wavelength laser.

- Wang, K., Huang, J. & Wei, Z. X. Conducting Polyaniline Nanowire Arrays for High Performance Supercapacitors. *J. Phys. Chem. C* **114**, 8062–8067 (2010).
- Yan, J. *et al.* Preparation of a graphene nanosheet/polyaniline composite with high specific capacitance. *Carbon* **48**, 487–493 (2010).
- Wang, D. W. *et al.* Fabrication of Graphene/Polyaniline Composite Paper via In Situ Anodic Electropolymerization for High-Performance Flexible Electrode. *ACS Nano* **3**, 1745–1752 (2009).
- Yun, Y. S. *et al.* Microporous Carbon Nanoplates from Regenerated Silk Proteins for Supercapacitors. *Adv. Mater.* **25**, 1993–1998 (2013).
- Zhang, L. *et al.* Porous 3D graphene-based bulk materials with exceptional high surface area and excellent conductivity for supercapacitors. *Sci. Rep.* **3**, 1408, (2013).
- Hu, C. C., Chang, K. H., Lin, M. C. & Wu, Y. T. Design and tailoring of the nanotubular arrayed architecture of hydrous RuO₂ for next generation supercapacitors. *Nano Lett.* **6**, 2690–2695 (2006).
- Yang, Q., Lu, Z., Sun, X. & Liu, J. Ultrathin Co₃O₄ nanosheet arrays with high supercapacitive performance. *Sci. Rep.* **3**, 3537 (2013).
- Fan, H. S., Zhao, N., Wang, H., Xu, J. & Pan, F. 3D conductive network-based free-standing PANI-RGO-MWNTs hybrid film for high-performance flexible supercapacitor. *J. Mater. Chem. A* **2**, 12340–12347 (2014).
- Meng, Y., Wang, K., Zhang, Y. & Wei, Z. X. Hierarchical Porous Graphene/ Polyaniline Composite Film with Superior Rate Performance for Flexible Supercapacitors. *Adv. Mater.* **25**, 6985–6990 (2013).
- Wang, Y.-G., Wang, Z.-D. & Xia, Y.-Y. An asymmetric supercapacitor using RuO₂/TiO₂ nanotube composite and activated carbon electrodes. *Electrochim. Acta* **50**, 5641–5646 (2005).
- Lee, B. J. *et al.* Carbon nanofibre/hydrous RuO₂ nanocomposite electrodes for supercapacitors. *J. Power Sources* **168**, 546–552 (2007).
- Pandolfo, A. G. & Hollenkamp, A. F. Carbon properties and their role in supercapacitors. *J. Power Sources* **157**, 11–27 (2006).
- Kim, K.-S. & Park, S.-J. Synthesis of carbon-coated graphene electrodes and their electrochemical performance. *Electrochim. Acta* **56**, 6547–6553 (2011).



14. Gavrilov, N. *et al.* High-performance charge storage by N-containing nanostructured carbon derived from polyaniline. *Carbon* **50**, 3915–3927 (2012).
15. Hu, Y. *et al.* Synthesis of self-supported non-precious metal catalysts for oxygen reduction reaction with preserved nanostructures from the polyaniline nanofiber precursor. *J. Power Sources* **225**, 129–136 (2013).
16. Silva, R., Voiry, D., Chhowalla, M. & Asefa, T. Efficient Metal-Free Electrocatalysts for Oxygen Reduction: Polyaniline-Derived N- and O-Doped Mesoporous Carbons. *J. Am. Chem. Soc.* **135**, 7823–7826 (2013).
17. Mo, Z., Peng, H., Liang, H. & Liao, S. Vesicular nitrogen doped carbon material derived from Fe₂O₃ templated polyaniline as improved non-platinum fuel cell cathode catalyst. *Electrochim. Acta* **99**, 30–37 (2013).
18. Guo, J., Chen, L., Wang, G., Zhang, X & Li, F. In situ synthesis of SnO₂-Fe₂O₃@ polyaniline and their conversion to SnO₂-Fe₂O₃ composite as fully reversible anode material for lithium-ion batteries. *J. Power Sources* **246**, 862–867 (2014).
19. Frackowiak, E., Gautier, S., Gaucher, H., Bonnamy, S. & Beguin, F. Electrochemical storage of lithium in multiwalled carbon nanotubes. *Carbon* **37**, 61–69 (1999).
20. Liu, C., Li, F., Ma, L.-P. & Cheng, H.-M. Advanced Materials for Energy Storage. *Adv. Mater.* **22**, E28–E62 (2010).
21. Fan, Z. J. *et al.* A Three-Dimensional Carbon Nanotube/Graphene Sandwich and Its Application as Electrode in Supercapacitors. *Adv. Mater.* **22**, 3723–3728 (2010).
22. Yang, S.-Y. *et al.* Design and tailoring of a hierarchical graphene-carbon nanotube architecture for supercapacitors. *J. Mater. Chem.* **21**, 2374–2380 (2011).
23. Xu, J. J., Wang, K., Zu, S. Z., Han, B. H. & Wei, Z. X. Hierarchical Nanocomposites of Polyaniline Nanowire Arrays on Graphene Oxide Sheets with Synergistic Effect for Energy Storage. *ACS Nano* **4**, 5019–5026 (2010).
24. Fan, H. S., Wang, H., Zhao, N., Zhang, X. L. & Xu, J. Hierarchical nanocomposite of polyaniline nanorods grown on the surface of carbon nanotubes for high-performance supercapacitor electrode. *J. Mater. Chem.* **22**, 2774–2780 (2012).
25. Fang, Y. *et al.* A Low-Concentration Hydrothermal Synthesis of Biocompatible Ordered Mesoporous Carbon Nanospheres with Tunable and Uniform Size. *Angew. Chem. Int. Edit.* **49**, 7987–7991 (2010).
26. Numao, S., Judai, K., Nishijo, J., Mizuuchi, K. & Nishi, N. Synthesis and characterization of mesoporous carbon nano-dendrites with graphitic ultra-thin walls and their application to supercapacitor electrodes. *Carbon* **47**, 306–312 (2009).
27. Zhang, J., Kong, L. B., Wang, B., Luo, Y. C. & Kang, L. In-situ electrochemical polymerization of multi-walled carbon nanotube/polyaniline composite films for electrochemical supercapacitors. *Synth. Met.* **159**, 260–266 (2009).
28. Li, L. *et al.* A doped activated carbon prepared from polyaniline for high performance supercapacitors. *J. Power Sources* **195**, 1516–1521 (2010).
29. Li, X., Zhang, H., Wang, G. & Jiang, Z. A novel electrode material based on a highly homogeneous polyaniline/titanium oxide hybrid for high-rate electrochemical capacitors. *J. Mater. Chem.* **20**, 10598–10601 (2010).
30. Yuan, D. S. *et al.* Nitrogen-enriched carbon nanowires from the direct carbonization of polyaniline nanowires and its electrochemical properties. *Electrochem. Commun.* **13**, 242–246 (2011).
31. Xiang, X. *et al.* Activated carbon prepared from polyaniline base by K(2)CO(3) activation for application in supercapacitor electrodes. *J. Solid State Electr.* **15**, 579–585 (2011).
32. Yang, M., Cheng, B., Song, H. & Chen, X. Preparation and electrochemical performance of polyaniline-based carbon nanotubes as electrode material for supercapacitor. *Electrochim. Acta* **55**, 7021–7027 (2010).
33. Kovtyukhova, N. I. *et al.* Layer-by-Layer Assembly of Ultrathin Composite Films from Micron-Sized Graphite Oxide Sheets and Polycations. *Chem. Mater.* **11**, 771–778 (1999).

Acknowledgments

N.Z. and J.X. thank the support of the National Natural Science Foundation of China (Grant No. 50821062, 21121001). H.S.F. and F.P. thank the support jointly by Shenzhen Science and Technology Research Grant (No. ZDSY20130331145131323, CXZZ20120829172325895, JCYJ20120614150338154).

Author contributions

H.S.F. designed and conducted the experiments. H.W. and N.Z. assisted with the experiments and the data analyses. J.X. and F.P. took part in discussion. This manuscript was written by H.S. F. All authors reviewed this manuscript.

Additional information

Competing financial interests: The authors declare no competing financial interests.

How to cite this article: Fan, H.S., Wang, H., Zhao, N., Xu, J. & Pan, F. Nano-porous architecture of N-doped carbon nanorods grown on graphene to enable synergetic effects of supercapacitance. *Sci. Rep.* **4**, 7426; DOI:10.1038/srep07426 (2014).



This work is licensed under a Creative Commons Attribution-NonCommercial-NoDerivs 4.0 International License. The images or other third party material in this article are included in the article's Creative Commons license, unless indicated otherwise in the credit line; if the material is not included under the Creative Commons license, users will need to obtain permission from the license holder in order to reproduce the material. To view a copy of this license, visit <http://creativecommons.org/licenses/by-nc-nd/4.0/>